Steady-state radiation ablation in the wire-array Z pinch

Edmund P. Yu,[a] B. V. Oliver, D. B. Sinars, T. A. Mehlhorn, and M. E. Cuneo
Sandia National Laboratories, P.O. Box 5800, Albuquerque, New Mexico 87185-1193

P. V. Sasorov
Institute of Theoretical and Experimental Physics, Moscow 117218, Russia

M. G. Haines and S. V. Lebedev
Blackett Laboratory, Imperial College, London SW7 2BW, United Kingdom

(Received 28 July 2006; accepted 18 December 2006; published online 20 February 2007)

The mass ablation phase of a wire-array Z pinch is investigated using steady-state (r,θ) simulations. By identifying the dominant physical mechanisms governing the ablation process, a simple scaling relation is derived for the mass ablation rate $\dot{m}$ with drive current I, in the case where radiation is the primary energy transport mechanism to the wire core. In order to investigate the dependence of $\dot{m}$ on wire core size, a simplified analytical model is developed involving a wire core placed in a heat bath and ablating due to radiation. Results of the model, simulation, and experiment are compared. © *2007 American Institute of Physics*. [DOI: 10.1063/1.2435332]

I. INTRODUCTION

A wire-array Z pinch is a cylindrical array of fine metal wires which, when pulsed with current, is subject to a radial $\mathbf{j}\times\mathbf{B}$ force which implodes the pinch. The resulting stagnation and thermalization of the pinch on the cylindrical axis of symmetry can yield x-ray powers in excess of 200 TW,[1–3] thus making the Z pinch an attractive radiation source for a number of applications, including inertial confinement fusion, high energy density plasmas, and laboratory astrophysics.[4–11] The use of wire arrays to initiate the Z-pinch implosion, as opposed to alternate Z-pinch loads (i.e., annular foils, gas puffs, foams), is of interest because arrays with larger numbers of wires ($\geqslant$100) can dramatically increase the x-ray power.[1] However, many elements of wire-array dynamics are still not well understood.

Originally, wire cores in a wire array were thought to vaporize due to Joule heating, merge, and implode as a thin plasma shell. Later, experiments revealed a much different picture:[12–15] early in the current pulse, a low density plasma forms around the wire cores, due perhaps to the desorption and ionization of contaminant hydrocarbons embedded within the cores.[16] This highly conductive plasma "corona" provides an alternate path through which current can flow, and effectively shunts current out of the cores. Consequently, rather than immediately vaporizing due to Joule heating, wires remain as dense cool cores, surrounded by hot, tenuous "coronal" plasma which carries the majority of the current. While wire cores carry little current and therefore remain stationary, the current-carrying corona is acted on by the $\mathbf{j}\times\mathbf{B}$ force and is swept radially inward towards the array axis, eventually accumulating there as a precursor pinch. However, the hot corona also acts to ablate (i.e., vaporize) mass off the wire cores, thereby replenishing the supply of coronal mass surrounding the wires. Thus, the lifetime of a wire-array Z pinch is dominated by a mass ablation phase, during which stationary wire cores continuously generate hot corona mass via the ablation process, which is subsequently swept towards the axis by the $\mathbf{j}\times\mathbf{B}$ force.

It is believed that the mass ablation phase ends when wire cores have run out of material at certain axial positions, and the ensuing implosion phase proceeds as a snowplow implosion, sweeping up all the prefill plasma which had been injected previously into the array interior. Since the mass ablation phase determines the radial redistribution of array mass prior to implosion, it is of critical importance in determining the timing and amplitude of the radiation pulse produced by the wire-array implosion. As has been argued in Ref. 14, it is believed that there is an optimum mass distribution for maximum radiation power.

In this paper we attempt to elucidate the physics of the mass ablation phase, which has been studied previously in the context of astrophysics[17] and inertial confinement fusion,[18–21] as well as in the wire-array Z-pinch setting.[14,22–24] The ablation process is in fact axially nonuniform,[13] but for the sake of simplicity we ignore this axial dependence and focus on *steady-state* ablation in the 2D (r,θ) plane. By interrogating wire-array simulations, we will gain intuition into the dominant physical mechanisms, and develop a simple analytic ablation model which agrees reasonably well with simulation. In particular we are interested in making a connection to the experimental observation that mass ablation rate appears to vary with wire core size,[25,26] as well as the ratio of the interwire gap to core size.[27] The origin of this dependence has been addressed theoretically by Sasorov,[28] in the limit in which the azimuthal width of the coronal plasma surrounding wire cores is much less than the interwire gap.

II. SIMULATION DESCRIPTION

Much of the work in this paper revolves around a suite of steady-state wire-array simulations, run using ALEGRA-HEDP,[29–31] a resistive magnetohydrodynamic

[a]Electronic mail: epyu@sandia.gov

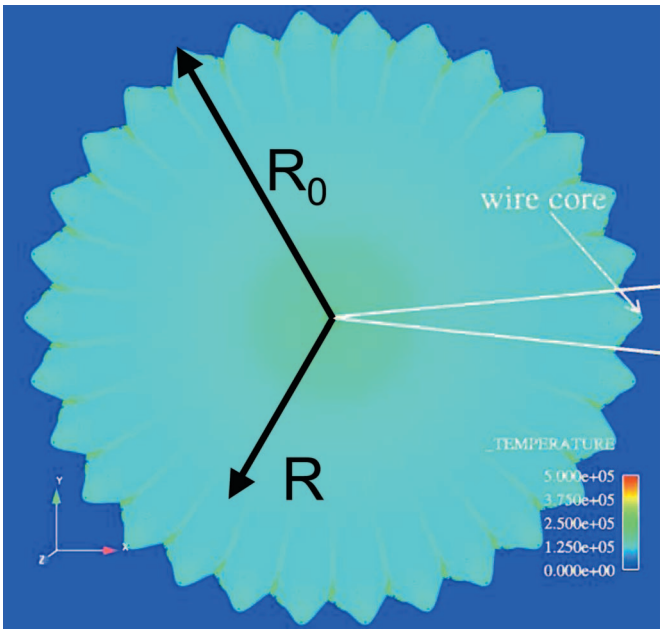

FIG. 1. (Color) (r,θ) simulation of an $N=30$, $R_0=0.01$ m wire array, with wire cores of radius $r_w=25$ μm. Note the presence of cold wire cores surrounded by hot plasma corona (the temperature scale is in units of Kelvin), which is continuously swept towards the array axis. In actuality, only a single wedge of the array is simulated, with periodic boundary conditions applied at the azimuthal boundaries (denoted by solid white lines). The inner boundary of the mesh, located at $R=1.0\times10^{-4}$ m, is rigid (i.e., reflective). Resolution is fairly high in and around the wire core (cell size 1 μm), in order to resolve the steep gradients which develop there.

(MHD) code developed at Sandia National Laboratories, which also includes thermal and radiative transport modeling. Although ALEGRA supports more advanced radiation transport methods (i.e., multigroup implicit Monte Carlo) and allows for separate ion and electron temperatures, all simulations here employ a single-group radiation diffusion model and assume equal ion and electron temperatures. As remarked earlier, wire-array dynamics are 3D in nature, but we restrict our simulations to the (r,θ) plane (see Fig. 1).

As pointed out by Chittenden,[23] ideal MHD wire-array simulations driven with a constant current eventually reach an equilibrium, with the exception of the precursor pinch region on axis, which is continually accumulating mass. In this paper we are interested in the physics of steady-state wire ablation, which will turn out to be determined by a thin layer surrounding the wire cores (see Sec. III A). All simulations are run with constant current drive. Furthermore, all arrays are of fixed radius $R_0=0.01$ m, and consist of tungsten wires of varying number N, and initial radius r_w. The simulations are initialized with a cold $(T=1450$ K) core at solid density $(\rho=1.93\times10^4$ kg/m$^3)$ of radius r_w (varying from 5 to 35 μm), surrounded by a hot $(T=4\times10^5$ K), low density $(\rho=0.19$ kg/m$^3)$ plasma corona, of radius $2r_w$. The equilibrium reached is insensitive to the initial conditions of the corona, which rapidly expands and is swept downstream towards the array axis, thereby establishing the equilibrium shown in Fig. 1. The core initial condition is probably unrealistically cool and dense. Recall that the cores carry all the current (and are therefore subject to Joule heating) until the formation of coronal plasma. Experimental images of tungsten cores reveal that, at this time, cores are heated sufficiently that they are no longer solid density objects, but rather comprise a complicated liquid droplet/vapor mixture.[32,33]

Although our core initial condition may be unrealistic, we are interested here less on simulating exact experimental conditions, and more on understanding the physics governing an idealized case of wire ablation, namely, the case of a hot corona ablating a stationary, cold core, which is acting solely as a mass source. To this end, the exact initial conditions of the core are not so important, so long as the temperature remains cool enough that the core does not begin to expand appreciably.

ALEGRA uses high fidelity equation of state tables[34] and electrical conductivity models (based on quantum molecular dynamic simulations[35]). In these simulations, however, we reduce the core electrical conductivity σ_c by a factor of 100, thereby artificially driving current completely out of the core. The reasons for this reduction are twofold. Although the corona carries the majority of current, if σ_c is left unmodified, the core carries enough current that the resulting Joule heating continuously increases the core temperature, causing it to expand and eventually vaporize. Such a time-varying condition is not compatible with our goal of achieving a steady state. A second reason for reducing σ_c stems from a comparison between experiment and simulation,[25,36] which suggests that in the unmodified simulations, cores vaporize (due to Joule heating) too early, and the resulting plasma shell implosion begins prematurely relative to experiment. Much better agreement with experiment, both in terms of the start of array implosion, as well as x-ray backlighting radiographs of the array taken during the mass ablation phase, is found by reducing σ_c by at least a factor of 10.

The physical reason for the need to reduce the core conductivity is open for debate. Since in reality tungsten cores consist of a liquid droplet/vapor mixture, a possible explanation is provided by percolation theory,[37] which states that once the average density of the mixture falls below $\rho_L/3$, where ρ_L is the liquid density, the mixture becomes a very poor conductor. The idea here is that the vapor separating liquid droplets is poorly conducting, whereas the droplets themselves constitute a "good" conductor. Consequently once the separation between droplets exceeds a critical value, a conducting path no longer exists between droplets.

Note that σ_c is effectively a knob by which we can explore two different limits of wire ablation. If σ_c is left unchanged, the dominant core ablation mechanism is Joule heating, and the entire volume of the core heats, expands, and vaporizes prematurely relative to experiment. Conversely, if σ_c is reduced by a factor of 100, Joule heating no longer plays a role in the core; the body of the core remains cool and unexpanded, while only the core surface experiences heating due to radiation transport from the surrounding hot plasma corona (electron thermal conduction is secondary to radiation transport, as we will show). In this paper, we will focus on this limit, in which the core functions only as a

passive mass source, slowly ablating due to radiation transport.

III. GENERAL LAYER PHYSICS

A. Resistive layer

In this section we begin consideration of the physics governing steady-state mass ablation, in the context of resistive MHD. The importance of nonideal MHD effects in the Z-pinch setting has been considered previously by Oliver and Mehlhorn.[38] Recall that the MHD Ohm's law

$$\mathbf{E}+\mathbf{v}\times\mathbf{B}=\eta\mathbf{j}, \tag{1}$$

coupled with Faraday's law and Ampére's law, yields the time variation of the magnetic field

$$\frac{\partial\mathbf{B}}{\partial t}=\nabla\times(\mathbf{v}\times\mathbf{B})+\frac{\eta}{\mu_0}\nabla^2\mathbf{B}, \tag{2}$$

where we have assumed the plasma resistivity η is spatially constant, for the sake of simplicity. All other variables in Eqs. (1) and (2) have their usual meaning, and SI units are used throughout. The first term on the right-hand side describes the usual convection of magnetic field with the plasma flow, a consequence of the plasma and field being frozen together in the ideal $(\eta\to 0)$ limit. The second term on the right-hand side of Eq. (2) describes how finite η breaks this frozen field constraint, and permits diffusion of the magnetic field through the plasma. Consider the ratio of terms $\nabla\times(\mathbf{v}\times\mathbf{B})/(\eta/\mu_0)\nabla^2\mathbf{B}$. For a system with a characteristic length scale L and characteristic plasma velocity v, this ratio can be expressed as a dimensionless quantity, the so-called magnetic Reynold's number:

$$R_M=\frac{\mu_0 vL}{\eta}. \tag{3}$$

Consequently a flow satisfying $R_M\gg 1$ is basically ideal MHD flow, whereas $R_M\ll 1$ corresponds to nonideal flow in which magnetic diffusion is dominant.

As has been described elsewhere,[14,23] the Z-pinch plasma can be divided into two regions. The first region encompasses most of the pinch, extending from the array axis out to nearly the array radius R_0. The scale length of the region is "large" $(L\sim R_0)$, and the typical velocity is "fast" (i.e., super-Alfvénic). Hence, $R_M\gg 1$ and the flow is essentially ideal. This region was studied in Refs. 23, 39, and 40; there it was found that the steady-state ideal MHD equations in the pressureless limit possess analytic solutions for $v>v_A$, where v_A is the Alfvén speed, but solutions break down at the trans-Alfvénic point, $v=v_A$, leading to a natural condition for the boundary of this first region.

This brings us to the second region, which constitutes a thin boundary layer near the wire cores, at $R\sim R_0$ (note that R measures distance from the array axis, as in Fig. 1). In this layer plasma is accelerated from zero velocity (as it leaves the core surface), up to the Alfvén speed. In this thin layer, the characteristic size is "small" and the characteristic velocity is "low" $(v<v_A)$, so $R_M\ll 1$, as was shown more rigorously in Ref. 41. Consequently nonideal (i.e., resistive) effects are important in the layer, which we henceforth refer to as the *resistive layer*. Since within the resistive layer the plasma satisfies $R_M\ll 1$, while in the bulk of the pinch $R_M\gg 1$, it is natural to expect that the transition between the two regions occurs at $R_M\sim 1$. From Eq. (3), this condition enables an estimate of the size δ of the resistive layer:

$$\delta\sim\frac{\eta}{\mu_0 v}. \tag{4}$$

For the case $R_0=0.01$ m, $N=300$, $I=3$ MA, $r_w=15$ μm, typical values for the resistivity and velocity in the resistive layer are $v\sim 2.5\times 10^4$ m/s and $\eta\sim 1.6\times 10^{-5}$ Ω m, which suggests $\delta\sim 0.5$ mm. Note that in Fig. 2, the resistive layer may be identified as the plasma region to the right of the contour C, and includes the much thinner "ablation layer," which will be discussed in the following section.

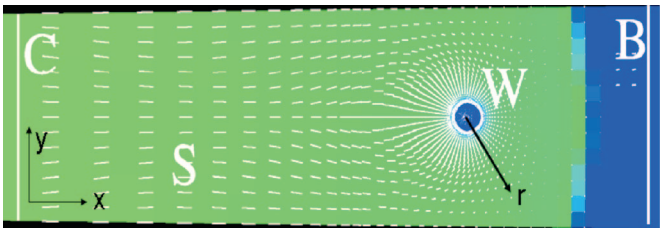

FIG. 2. (Color) Resistive layer region for $r_w=15$ μm, $N=300$, $I=3$ MA. Recalling that we only simulate a single periodic wedge of the entire array (see Fig. 1), this figure focuses on that region of the wedge near the wire core. The contour C lies at $R=9.5$ mm, 0.5 mm downstream of the wire core and approximately the trans-Alfvénic point (and hence the inner boundary of the resistive layer), W denotes the wire boundary ($T=1.5\times 10^4$ K contour), and B denotes the outer boundary of the region, which lies in the vacuum region outside the array. The surface S encompasses the region in the x-y plane between contours C and B, excluding the wire core region enclosed within contour W. Also plotted are plasma flow velocity vectors.

In this paper we focus on the physics of wire ablation. As was pointed out by Sasorov,[14] we can address this problem by restricting attention to the resistive layer. We now attempt to elucidate the general physics of the resistive layer by application of the steady-state conservation laws of mass, momentum, and energy. As noted in Ref. 14, the resistive layer, being thin compared to the array radius, can be approximated in the Cartesian sense, with coordinate x playing the role of R, the radial distance from the array axis. Application of the MHD momentum equation

$$\rho\left(\frac{\partial\mathbf{v}}{\partial t}+\mathbf{v}\cdot\nabla\mathbf{v}\right)=-\nabla p+\mathbf{j}\times\mathbf{B} \tag{5}$$

to the steady-state, 1D Cartesian case yields

$$\rho v\frac{dv}{dx}=-\frac{dp}{dx}-\frac{d}{dx}\left(\frac{B^2}{2\mu_0}\right), \tag{6}$$

where we have assumed a purely "azimuthal" global magnetic field $\mathbf{B}=B\hat{y}$, and ρ and p represent the plasma mass density and pressure, respectively. Since ρv is a spatial constant, by steady-state mass conservation, Eq. (6) can be integrated to yield a magnetic Bernoulli-type equation:

$$\rho v^2 + p + \frac{B^2}{2\mu_0} = \frac{B_0^2}{2\mu_0}, \tag{7}$$

where we have assumed at the core surface, $B=B_0$, $v=0$, and $p=0$. We can derive an order of magnitude estimate on the characteristic plasma velocity in the resistive layer by noting from simulation that the resistive layer carries a significant fraction of the total current. In the limit in which the resistive layer carries nearly *all* the current, at the inner edge of the resistive layer, $B \simeq 0$ from Ampére's law. Coupled with the fact that p is small compared to the magnetic pressure, except very near the core, Eq. (7) yields

$$\rho v^2 \simeq \frac{B_0^2}{2\mu_0}, \tag{8}$$

i.e., the characteristic velocity in the resistive layer is Alfvénic, as is reasonable:

$$v \sim \frac{B_0}{\sqrt{\mu_0 \rho}} \sim v_A. \tag{9}$$

Let us now consider the full MHD energy equation

$$\frac{\partial}{\partial t}\left(\rho e + \frac{1}{2}\rho v^2\right) + \nabla \cdot \left[\left(\rho e + \frac{1}{2}\rho v^2 + p\right)\mathbf{v} - \kappa \nabla T + \mathbf{S}\right] = \mathbf{E} \cdot \mathbf{j}, \tag{10}$$

where e is the internal energy per unit mass, $\mathbf{S}$ is the energy flux due to radiation transport, κ is the thermal conductivity, and $\mathbf{E}\cdot\mathbf{j}$ is the electrical power imparted to the system. It is enlightening to integrate Eq. (10) over the resistive layer surface S, as shown in Fig. 2, which will permit us to examine all the different energy fluxes into and out of the resistive layer:

$$\int_S \mathbf{E}\cdot\mathbf{j}dS = \int_S \frac{\partial}{\partial t}\left(\rho e + \frac{1}{2}\rho v^2\right)dS + \int_C \left(\rho h + \frac{1}{2}\rho v^2\right)\mathbf{v}\cdot\mathbf{n}dl - \int_C \kappa \nabla T \cdot \mathbf{n}dl + \int_C \mathbf{S}\cdot\mathbf{n}dl + \int_B \mathbf{S}\cdot\mathbf{n}dl + \int_W \left(\rho h + \frac{1}{2}\rho v^2\right)\mathbf{v}\cdot\mathbf{n}dl - \int_W \kappa \nabla T \cdot \mathbf{n}dl + \int_W \mathbf{S}\cdot\mathbf{n}dl. \tag{11}$$

In the above equation, $\mathbf{n}$ represents a unit vector normal to the contour of interest and pointing outwards from the surface S, and dl is a line element lying along the contour. Also, we have introduced the specific enthalpy h:

$$h = e + \frac{p}{\rho}. \tag{12}$$

Figure 3 plots the magnitude of the dominant terms. The dominant power input into the resistive layer is the electrical power $\int_S \mathbf{E}\cdot\mathbf{j}dS$, and the dominant power output balancing the electrical power is the convective term $\int_C (\rho h + \frac{1}{2}\rho v^2)\mathbf{v}\cdot\mathbf{n}dl$, i.e.,

$$\int_S \mathbf{E}\cdot\mathbf{j}dS \sim \int_C \left(\rho h + \frac{1}{2}\rho v^2\right)\mathbf{v}\cdot\mathbf{n}dl. \tag{13}$$

The gradual temporal decay in $\int_S \mathbf{E}\cdot\mathbf{j}dS$ can be associated with the diffusion of magnetic field through the resistive layer. We have neglected to plot the energy transported to the core via radiation $(\int_W \mathbf{S}\cdot\mathbf{n}dl)$ and thermal conduction $(-\int_W \kappa\nabla T\cdot\mathbf{n}dl)$, as well as the term $\int_W (\rho h + \frac{1}{2}\rho v^2)\mathbf{v}\cdot\mathbf{n}dl$, which are in fact negligible compared to the electrical power and convective terms, and consequently will not play a role in the overall determination of the resistive layer temperature.

We can be even more specific about the dominant energy balance in the resistive layer by noting from Eq. (1),

$$\mathbf{E}\cdot\mathbf{j} = \eta j^2 + \mathbf{v}\cdot(\mathbf{j}\times\mathbf{B}). \tag{14}$$

Consequently Eq. (13) can be written as

$$\int_S \eta j^2 dS + \int_S \mathbf{v}\cdot(\mathbf{j}\times\mathbf{B})dS \sim \int_C \rho h \mathbf{v}\cdot\mathbf{n}dl + \int_C \frac{1}{2}\rho v^2 \mathbf{v}\cdot\mathbf{n}dl. \tag{15}$$

We must point out that the approximate balance represented in Eq. (15) is relevant only to high wire number arrays (i.., $N \geqslant 300$), where, due to the small interwire gap, the cores and relatively dense surrounding corona effectively play the role of a hohlraum wall, thus trapping radiation inside the array. As N decreases and the interwire gap increases, the array acts as more of a "leaky" hohlraum. Consequently, radiation flow out of the array becomes more important and must be included in Eq. (15).

Using $j \sim B_0/\mu_0\delta$, coupled with Eqs. (4) and (9), we find that the first, second, and fourth terms in Eq. (15) can be estimated to have the same order of magnitude $B_0^2 R_0 v/\mu_0$ (recall that R_0 represents the array radius). In fact, as can be inferred from Fig. 3, simulation suggests all four terms in Eq. (15) are of the same order of magnitude, permitting us to obtain an estimate of the enthalpy by balancing the convective enthalpy term $(\int_C \rho h \mathbf{v}\cdot\mathbf{n}dl)$ with any of the remaining three terms: $\rho h v R_0 \sim B_0^2 R_0 v/\mu_0$. Hence, the overall enthalpy of the resistive layer is on order the magnetic energy density,

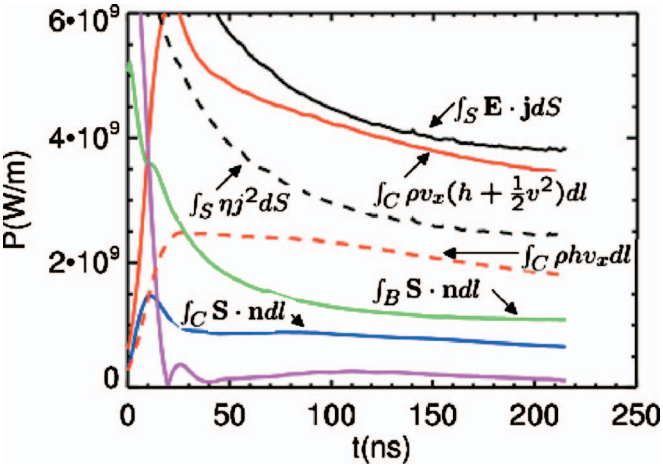

FIG. 3. (Color) Magnitude of dominant power flows into and out of the resistive layer, for $r_w=15$ μm, $N=300$, $I=3$ MA. Since we only simulate a single periodic 2D (r,θ) wedge, all powers are measured per unit axial length of the array, and furthermore must be multiplied by N, the number of wires, to obtain the value relevant to the entire array. The components shown are electrical power deposited within the resistive layer $\int_S \mathbf{E}\cdot\mathbf{j}dS$ (solid black), enthalpy and kinetic energy convected out $\int_C \rho v_x(h+\frac{1}{2}v^2)dl$ (solid red), radiation flux out $\int_B \mathbf{S}\cdot\mathbf{n}dl$ (green), radiation flux in $\int_C \mathbf{S}\cdot\mathbf{n}dl$ (blue), and $|\partial/\partial t\int(\rho e+\frac{1}{2}\rho v^2)dS|$ (magenta). We also plot $\int_S \eta j^2 dS$ (black dashed) and $\int_C \rho h v_x dl$ (red dashed). In fact the current is ramped up over a period of 40 ns to its target steady-state value; the time at which this value is reached is defined as $t=0$.

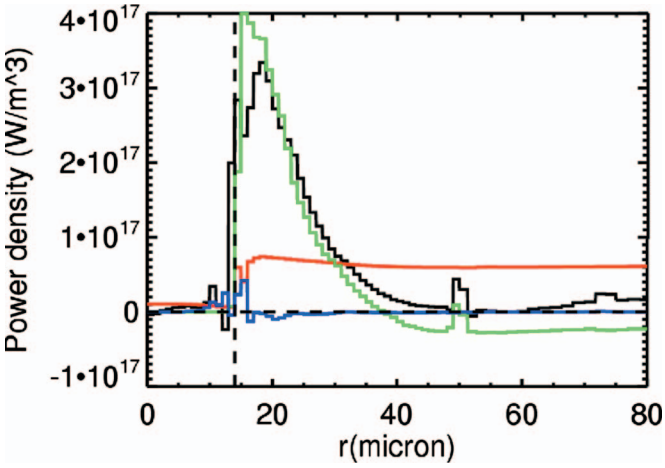

FIG. 4. (Color) Divergence of energy flows for $r_w=15$ μm, $N=300$, $I=3$ MA. The components are $\mathbf{E}\cdot\mathbf{j}$ (red), $\nabla\cdot(\rho h+\frac{1}{2}\rho v^2)\mathbf{v}$ (black), $-\nabla\cdot\mathbf{S}$ (green), and $\nabla\cdot\kappa\nabla T$ (blue). As in Fig. 2, r represents distance from the core center. To be precise, these values are computed along a lineout extending from the core center and oriented in the $\hat{y}$ direction. The dashed vertical line denotes the location of the core surface, which has ablated down to $r=14$ μm. These profiles, as well as all subsequent profiles, are shown at a time at which $\dot{m}$ has reached its equilibrium value.

$$h(\rho,T)\sim\frac{B_0^2}{\mu_0\rho}. \tag{16}$$

Note that all of the main relations so far, Eqs. (4), (9), and (16), were found in Ref. 14.

B. Ablation layer

Up to this point, we have not mentioned the actual ablation mechanism. To address this, we will study the dominant energy transfer close to the core. We rewrite the steady-state energy equation:

$$\nabla\cdot\left[\left(\rho h+\tfrac{1}{2}\rho v^2\right)\mathbf{v}-\kappa\nabla T+\mathbf{S}\right]=\mathbf{E}\cdot\mathbf{j}. \tag{17}$$

Close to the core there exists a region of approximate cylindrical symmetry in which $\mathbf{v}\simeq v_r\hat{r}$ (see Fig. 2), and ρ, v_r, T are approximately functions only of r, the radial distance from the core center (although $\mathbf{B}$ and j_z will not possess this symmetry). In Fig. 4 we plot the terms in the above equation, as a function of r, and find that the rate at which energy is imparted to the plasma electrically $(\mathbf{E}\cdot\mathbf{j})$ and via thermal conduction $(-\nabla\cdot\kappa\nabla T)$ is secondary. In a thin layer ($\approx$20 μm) near the wire core, which we will henceforth refer to as the *ablation layer*, the dominant heating mechanism is in fact radiation $(\nabla\cdot\mathbf{S})$, which is in turn balanced by the dominant cooling mechanism, convective energy flow $\left[\left(\rho h+\frac{1}{2}\rho v^2\right)\mathbf{v}\right]$.

Consequently, in the ablation layer, the energy equation reduces to

$$\nabla\cdot\left[\left(\rho h+\tfrac{1}{2}\rho v^2\right)\mathbf{v}+\mathbf{S}\right]\simeq 0, \tag{18}$$

which, using cylindrical symmetry, reduces to

$$r\left[\left(\rho h+\tfrac{1}{2}\rho v^2\right)v_r+S_r\right]\simeq\text{const}. \tag{19}$$

As will be argued in the next section, the constant vanishes, yielding

$$\left(\rho h+\tfrac{1}{2}\rho v^2\right)v_r+S_r\simeq 0. \tag{20}$$

In Fig. 5 we plot these two terms, as well as the heat flux due to thermal conduction. Note that close to the core, there is indeed a region where the radiation flux is balancing the convective energy flux. Note also that the above two terms are very small at the core surface, which explains why we were able to ignore $\int_W(\rho h+\frac{1}{2}\rho v^2)\mathbf{v}\cdot\mathbf{n}dl$ and $\int_W\mathbf{S}\cdot\mathbf{n}dl$ in going from Eq. (11) to Eq. (13). However, both terms rapidly increase as we move away from the core surface, allowing

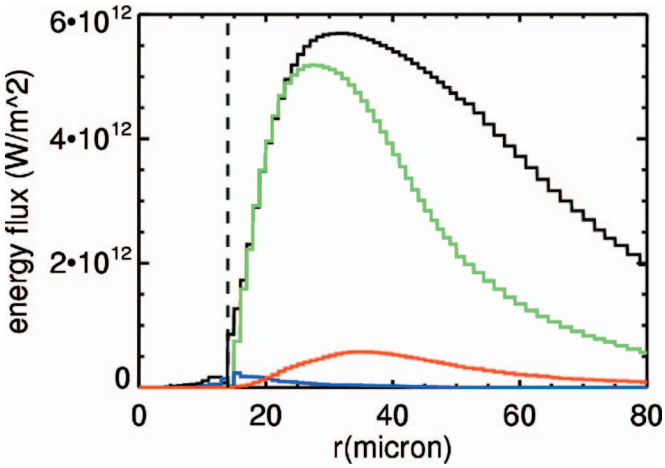

FIG. 5. (Color) Energy fluxes near the wire core, for $r_w=15$ μm, $N=300$, $I=3$ MA. The components are convective energy flux $(\rho h+\frac{1}{2}\rho v^2)v_r$ (black), radiation flux $-S_r$ (green), thermal conduction flux $\kappa dT/dr$ (blue), and kinetic energy flux $(\frac{1}{2}\rho v^2)v_r$ (red). The dashed vertical line represents the location of the core surface.

them to become the dominant terms in the energy equation within the ablation layer.

Since the contribution to the convective energy flux from kinetic energy $(\frac{1}{2}\rho v^3)$ is relatively small, Eq. (20) further reduces to

$$\rho h v_r \simeq -S_r. \tag{21}$$

In the limit that the corona is optically thick enough that it radiates like a black body, $-S_r \sim \sigma T^4$, where T is a characteristic temperature of the corona and σ is the Stefan-Boltzmann constant, we obtain our final relation governing ablation physics in the layer

$$\rho h(\rho,T) c_s(\rho,T) \sim \sigma T^4. \tag{22}$$

In the above equation we have noted that within the ablation layer, the plasma velocity is of order the sound speed c_s. We can justify this estimate by noting that within the ablation layer, the magnetic pressure varies little (its characteristic scale length being the much larger resistive layer). Consequently, from Eq. (7), we see that the increase in ρv^2 is balanced by a decrease in p, implying $v \sim c_s$. Note that there are 3 length scales for variations in v: (1) the ablation layer near the core, over which v is accelerated (by pressure) to on order the sound speed, (2) the resistive layer over which v is accelerated to the Alfvén velocity, and finally (3) the remaining bulk of the array, roughly of size R_0 (the array radius), over which the flow is accelerated to super-Alfvénic speeds.

C. Scaling with current drive *I*

Note that, given explicit expressions for $c_s(\rho,T)$ and $h(\rho,T)$, Eqs. (9), (16), and (22) constitute three equations in the four unknowns ρ, v, T, B_0, which are to be interpreted as values "characteristic" of the corona in the resistive layer. Consequently, we can express ρ, v, T in terms of B_0, which is in turn linearly related to the drive current I via $B_0 \sim \mu_0 I/2\pi R_0$. Hence we can find how typical values of the corona density, velocity, and temperature scale with the current drive I.

To this end, we adopt an expression for the specific enthalpy from Ref. 18,

$$h = h_0 \rho^{-0.14} T^{1.6}, \tag{23}$$

which produces good agreement with our simulation, and also assume

$$c_s = c_0 T, \tag{24}$$

which is consistent with the observation (from simulation) that $1+Z \sim T$, where Z represents the ionization state of the plasma. In Eqs. (23) and (24), h_0 and c_0 are constants, where $h_0 = 2.1\ \mathrm{J/kg(kg/m^3)^{0.14}(1/K^{1.6})}$ and $c_0 = 0.05\ \mathrm{m/s(1/K)}$. Using Eqs. (23) and (24), Eqs. (9), (16), and (22) yield the following scaling relations:

$$\rho \sim B_0^{1.09}, \tag{25}$$

$$T \sim B_0^{0.67}, \tag{26}$$

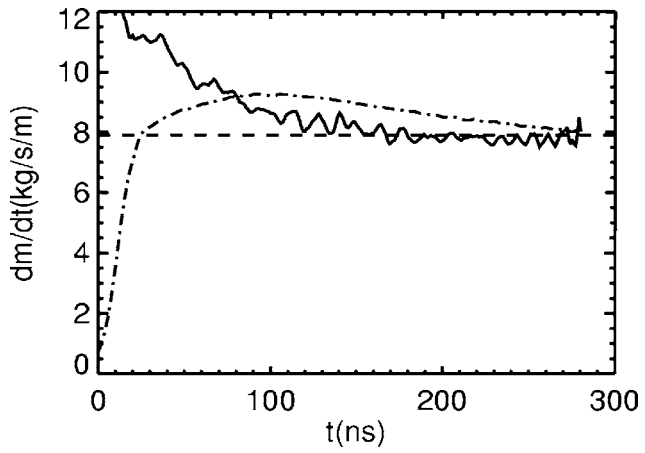

FIG. 6. Plot of $-\dot{m}_{\mathrm{wire}}$ (solid) and $\dot{m}_C$ (dashed-dotted) for $N=300$, $r_w = 15\ \mu\mathrm{m}$, $I=3$ MA. The steady-state value is denoted by the dashed line. Note the ablation rates here are representative of a single wire; to obtain the total ablation rate we must multiply by N.

$$v \sim B_0^{0.46}. \tag{27}$$

Note that scaling relations were obtained previously by Sasorov,[14] in the case where electron thermal conduction, rather than radiation transport, is the dominant heating mechanism. Recall that Eqs. (25)–(27) predict how "characteristic" values of ρ, v, T in the corona scale with global magnetic field B_0, or equivalently, drive current I (for fixed array radius R_0). Comparing these scaling predictions with simulation is nontrivial because all three variables vary spatially over the resistive layer, and it is not clear which value to use as our "characteristic" value.

One quantity which *is* spatially constant is the mass ablation rate $\dot{m}_C = \int_{C(R)} \rho \mathbf{v} \cdot \mathbf{n} dl$, where C is a contour downstream of the wire, located at fixed R (see Fig. 2), $\mathbf{n}$ is a unit vector normal to C, and dl is a differential line element lying along C. Note that physically $\dot{m}_C$ measures the mass per unit time (per unit axial length of the pinch) flowing through the contour C. In the steady state, $\dot{m}_C$ must be independent of the contour location R, by mass conservation, i.e., to avoid mass build up (or loss), the flux of mass entering and leaving a region must be equal.

Figure 6 plots $\dot{m}_C$ for the contour C fixed at $R = 9.5$ mm. In addition, we plot an alternative measure of the ablation rate $\dot{m}_{\mathrm{wire}}$, defined as the rate at which the wire core is losing mass due to ablation. Here, we define the wire core as any cold material satisfying $T < 1.5 \times 10^4$ K, roughly the critical point for tungsten. In Fig. 2, any mass contained within the boundary W is considered core material. Note that, as we would expect, in equilibrium the rate at which mass is burning off the wire, $\dot{m}_{\mathrm{wire}}$, is equal to the rate at which mass is flushed downstream, i.e., $-\dot{m}_{\mathrm{wire}} = \dot{m}_C \equiv \dot{m}$. The steady-state value $\dot{m}$ is denoted by the dashed line. Note that equilibrium cannot be maintained forever; material is continually stagnating on the array axis and eventually begins to affect plasma conditions near the cores.

Since $\dot{m} \sim 2\pi\rho v R_0/N$, from Eqs. (25) and (27) we can obtain the scaling for the mass ablation rate with global magnetic field B_0:

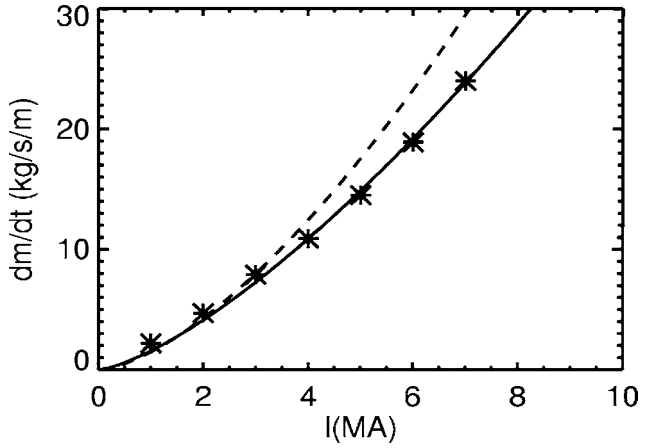

FIG. 7. Scaling of the mass ablation rate for a single wire, $\dot{m}$, with I, in the case $N=300$, $r_w=15$ μm. The crosses are simulation results, while the dashed line represents $\dot{m}\sim I^{1.55}$, the prediction from our scaling relations. A better fit is provided by the solid line, $\dot{m}\sim I^{1.4}$.

$$\dot{m} \sim B_0^{1.55} \sim I^{1.55}, \tag{28}$$

where in the last relation we have assumed R_0 is fixed. In Fig. 7 we compare this scaling with the results of constant current simulations, where array radius R_0 was held fixed. It appears that this predicted scaling is too strong, but nonetheless fairly close to the scaling produced by simulation. Note that the scaling in Eq. (28) depends fairly sensitively on the exponents used in the constitutive relations (23) and (24).

IV. SIMPLE ABLATION MODEL

In the previous section we outlined the dominant physics governing the resistive layer. There we found the existence of an even thinner region surrounding the core, the ablation layer, where the global magnetic field is of secondary importance. Namely, the flow is approximately cylindrically symmetric, implying $\mathbf{j}\times\mathbf{B}$ is dominated by ∇p in the momentum equation, and the magnetic field (or more specifically Joule heating) is also secondary in the dominant energy balance, which primarily involves radiation transport and convective enthalpy flux.

Consider the possibility that the ablation rate is governed solely by the physics in this thin region of cylindrical symmetry. In this case we can gain considerable insight by switching our attention away from the problem of a wire ablating in a wire array, and focusing instead on the far simpler problem of a cylindrical core embedded in a heat bath and ablating due to radiation. This reduced problem is also cylindrically symmetric and is free of the complication of a magnetic field. We assume that far from the core the heat bath is maintained at temperature T_0, i.e.,

$$T(r\to\infty)=T_0. \tag{29}$$

In this picture the role of $\mathbf{B}$ is to determine the temperature T_0, which, being a characteristic temperature of the plasma corona, will scale with magnetic field as in Eq. (26).

Let us now attempt to determine the mass ablation rate for the reduced problem described above, delaying justification of its relevance to Sec. V. To reiterate, we consider the case of a cold ($T=0$) cylindrical core of radius r_w, placed in a large heat bath, with the ablated plasma surrounding the core satisfying the boundary condition (29). As usual, we will limit ourselves to steady state. In the absence of electrical current the full energy equation (10) reduces to

$$\nabla\cdot\left[\left(\rho h+\tfrac{1}{2}\rho v^2\right)\mathbf{v}+\mathbf{S}\right]=0, \tag{30}$$

where we have assumed radiation conduction is dominant over electron thermal conduction. As demonstrated in the Appendix, this is a reasonable assumption for densities and temperatures of interest. Assuming cylindrical symmetry and $h\gg\frac{1}{2}v^2$ (a good approximation near the core, as evidenced by Fig. 5), Eq. (30) simplifies to

$$\frac{\dot{m}}{2\pi}h+rS_r=\text{const}, \tag{31}$$

where the constant will be shown to be zero. Here we have introduced the mass ablation rate $\dot{m}\equiv 2\pi\rho v_r r$, which we can identify as the mass per unit time (per unit axial length of the core) crossing through a circular contour of radius r. Note that the equation of mass conservation, in the steady-state limit and applied to a cylindrically symmetric system, yields

$$\rho v_r r=\text{const}, \tag{32}$$

so that $\dot{m}$ is a spatial constant. Now, Eq. (31) is basically the same as Eq. (21), derived in the previous section, and the interpretation remains the same: the radiation flux towards the core (rS_r) is balanced by the convective enthalpy flux away from the core ($\dot{m}h/2\pi$).

Ultimately we would like to integrate Eq. (31), which requires an explicit expression for the radiation flux $\mathbf{S}$. We adopt the radiation diffusion approximation

$$\mathbf{S}=-\frac{lc}{3}\nabla U, \tag{33}$$

where l is the Rosseland mean free path and U is the radiation energy density, which is sometimes used to define a radiation temperature T_r:

$$U\equiv\frac{4\sigma T_r^4}{c}, \tag{34}$$

where σ is the Stefan-Boltzmann constant. Strictly speaking the diffusion approximation holds only in the limit in which the plasma corona surrounding the core is optically thick, and U changes slightly over distances of order the mean free path l. In fact, from our wire-array simulations, the resistive layer is reasonably optically thick for high wire number, i.e., the optical depth $\int dx/l\sim 3$ for $N=300$, where the integral is taken across the layer, not including the core of course (note that l is of order 100 μm in the integral and throughout the bulk of the resistive layer). However, U increases very rapidly near the core, on order distances ~ 10 μm, which is also roughly the mean free path there. Consequently the limits of the diffusion approximation are strained at the core/corona interface. Nonetheless as a rule of thumb, even in such cases the diffusion approximation yields qualitatively correct results.[42]

Returning to our reduced problem, in general the mean free path l, as well as the enthalpy h, are functions of both temperature and density

$$h = h_0 \rho^m T^n, \tag{35}$$

$$l = l_0 \rho^\alpha T^\beta, \tag{36}$$

where h_0 and l_0 are constants, and typical values for the exponents are $m=-0.14$, $n=1.6$, $\alpha=-1.3$, $\beta=1.5$ [note that for this value of α and β, $l_0 \approx 3\times 10^{-11}$ m$(\mathrm{kg/m^3})^{1.3}$ $\mathrm{K}^{-1.5}$].[18] It follows that the boundary condition $T(r_w)=0$ implies $h(r_w)=S_r(r_w)=0$, so that the constant in Eq. (31) vanishes. Substituting Eq. (33) into Eq. (31), the energy equation becomes

$$\frac{\dot m}{2\pi} h(\rho,T) = \frac{rl(\rho,T)c}{3}\frac{dU}{dr}. \tag{37}$$

To obtain a rigorous solution of the problem, we must simultaneously solve the steady-state equation of radiation transport

$$\nabla\cdot\mathbf{S} = \frac{c}{l}(U_p - U), \tag{38}$$

where

$$U_p = \frac{4\sigma}{c}T^4 \tag{39}$$

is the equilibrium radiation energy density, as well as the steady-state momentum equation

$$\rho v_r \frac{dv_r}{dr} = -\frac{dp(\rho,T)}{dr}, \tag{40}$$

and steady-state equation of mass conservation (32), which constitute four equations in four unknowns (ρ, v_r, T, U). Obtaining an analytic solution to this system of equations may not be possible, so we instead focus our efforts on integrating Eq. (37), using approximations garnered from simulation.

It is tempting to assume a state of local thermodynamic equilibrium (LTE) between the radiation and plasma: $U \simeq U_p$, or equivalently $T \simeq T_r$ [from Eqs. (34) and (39)], which effectively allows us to discard Eq. (38), since U has been expressed in terms of T. However, such an approximation only holds when T varies slowly over a mean free path l, which is not the case near the core. Furthermore $U \simeq U_p$ implies $\nabla\cdot\mathbf{S}=0$, from Eq. (38), and consequently from Eq. (31), $dh/dr=0$. In fact h is a strongly varying function of r, owing to the rapid increase in T away from the core (cf. Fig. 9), thus invalidating the assumption $U \simeq U_p$. Physically we expect that near the core, $U > U_p$, so that $\nabla\cdot\mathbf{S} < 0$, meaning that there is a net flux of photons into the region, consistent with radiative heating of the corona. This heating is balanced by a cooling of the region convectively, i.e., $\nabla\cdot(\rho h\mathbf{v}) > 0$.

Although we cannot assume $U \simeq U_p$, and consequently $T \simeq T_r$, we can get a very rough relation between T and T_r by considering the energy equation (31) $\dot m h/2\pi = -rS_r$ in the limit in which all photons are traveling towards the core. Such an approximation is justified sufficiently close to the core, where very few photons are traveling radially outward (the core being too cold to radiate significantly), and most photons, having been "born" in hot regions further from the core, are travelling radially inwards towards the core. In this limit, the radiation flux is related very simply to the radiation energy density via the beam-like relation $S \simeq -cU/2$.[42] Consequently, the energy equation can be written

$$\frac{\dot m}{2\pi} h(\rho,T) \simeq r\frac{cU}{2}. \tag{41}$$

Recalling that $U=4\sigma T_r^4/c$ and adopting the dependence of the enthalpy h on density and temperature as in Eq. (23), we obtain a relation between T and T_r:

$$T_r \simeq \left(\frac{\dot m h_0}{4\pi\sigma}\right)^{1/4} \frac{T^{0.4}}{r^{1/4}\rho^{0.035}}, \tag{42}$$

where the term enclosed in parentheses is a spatial constant. If we were to ignore the relatively weak dependence on ρ and r, we can conclude $T_r \sim T^{0.4}$. In fact, from simulation, a better fit is provided by

$$T_r = T_{r0} T^\gamma, \tag{43}$$

where $\gamma=0.6$ (regretfully we offer no physical justification for this value) and T_{r0} is a constant (see Fig. 9).

Assuming that T_r is related to T as in Eq. (43), the energy equation (37) reduces to

$$\tilde{\dot m}\rho^{m-\alpha}\frac{1}{r} = \frac{dT^{\beta-n+4\gamma}}{dr}, \tag{44}$$

where we have introduced $\tilde{\dot m}$, which is different from $\dot m$ only by a constant factor:

$$\tilde{\dot m} = \frac{3(\beta-n+4\gamma)h_0}{16T_{r0}^4 l_0 \sigma\gamma}\frac{\dot m}{2\pi}. \tag{45}$$

Ultimately we are interested in the mass ablation rate $\dot m$ and its dependence on the wire size r_w, the bath temperature T_0, and details of the density profile. If the density profile were known, we could obtain $\dot m$ by integrating Eq. (44) from $r=r_w$ to $r\to\infty$ and using the boundary conditions $T(r_w)=0$ and $T(r\to\infty)=T_0$. In other words, the mass ablation rate is determined by the boundary conditions of the problem and is thus an *eigenvalue* of Eq. (44), as has been noted previously.[14,17]

Due to ρ being unknown, we cannot perform this integration, but note that if it were not for the density dependence, we could not satisfy our boundary condition $T(r\to\infty)=T_0$. Indeed, in the case $\rho=\rho_0=$const, the solution of Eq. (44) yields

$$T = [\tilde{\dot m}\rho_0^{m-\alpha}\ln(r/r_w)]^{1/\beta-n+4\gamma}, \tag{46}$$

which diverges as $r\to\infty$.

Now, rather than attempting to solve the coupled energy, radiation, and momentum equations in order to obtain a density profile, we instead consider the "reasonable" profile, valid in the plasma region $r > r_w$,

$$\rho = \frac{\rho_0}{\left(\frac{r-r_w}{s}\right)^{\mu}}, \tag{47}$$

where s is an arbitrary fixed length and $\rho_0 \equiv \rho(r_w+s)$. This profile has the undesired property that it diverges as $r \to r_w$, but it is nonetheless seen to provide an excellent fit to the simulation (see Fig. 10). With such a profile, integration of Eq. (44) leads to an integral of the form

$$\int_{r_w+\epsilon}^{\infty} \frac{dr}{(r-r_w)^{\nu} r}. \tag{48}$$

Note that we integrate from $r=r_w+\epsilon$, rather than $r=r_w$, so as to avoid the singularity in Eq. (47). In the case $\nu>0$, Eq. (48) can be evaluated in closed form[43]

$$\int_{r_w+\epsilon}^{\infty} \frac{dr}{(r-r_w)^{\nu} r} = \frac{1}{\nu \epsilon^{\nu}} F\left(1, \nu; 1+\nu; -\frac{r_w}{\epsilon}\right), \tag{49}$$

where F is the hypergeometric function. In the case $0<\nu<1$, the integral converges in the limit $\epsilon \to 0$, resulting in

$$\int_{r_w}^{\infty} \frac{dr}{(r-r_w)^{\nu} r} = \frac{\pi}{r_w^{\nu} \sin \nu\pi}. \tag{50}$$

If $\nu>1$ we note that in the limit $r_w/\epsilon \gg 1$, we can use the asymptotic relation[44]

$$F\left(1, \nu; 1+\nu; -\frac{r_w}{\epsilon}\right) \approx \frac{\epsilon}{r_w} F(1,1;1+\nu;1). \tag{51}$$

Noting that, for $\nu>1$,

$$F(1,1;1+\nu;1) = \frac{\Gamma(1+\nu)\Gamma(\nu-1)}{\Gamma(\nu)^2}, \tag{52}$$

where Γ is the gamma function, and also that $\Gamma(1+\nu) = \nu\Gamma(\nu)$, we finally obtain the result

$$\int_{r_w+\epsilon}^{\infty} \frac{dr}{(r-r_w)^{\nu} r} \approx \frac{1}{\epsilon^{\nu-1}(\nu-1) r_w}. \tag{53}$$

This approximation is valid for $\nu>1$ and ϵ small (i.e., $r_w/\epsilon \gg 1$) but *finite*. Consequently, substitution of Eq. (47) into Eq. (44), integrating from $r=r_w+\epsilon$ to $r \to \infty$, and applying the boundary conditions $T(r \to \infty)=T_0$ and $\lim_{\epsilon \to 0} T(r_w+\epsilon)=0$ yields, for $\mu(m-\alpha)>1$,

$$\tilde{\dot{m}} \approx \frac{T_0^{\beta-n+4\gamma}(\mu(m-\alpha)-1) r_w \epsilon^{\mu(m-\alpha)-1}}{\rho_0^{m-\alpha} s^{\mu(m-\alpha)}}, \tag{54}$$

while in the case $0<\mu(m-\alpha)<1$,

$$\tilde{\dot{m}} = \frac{T_0^{\beta-n+4\gamma} r_w^{\mu(m-\alpha)}}{\rho_0^{m-\alpha} s^{\mu(m-\alpha)}} \frac{\sin(\mu(m-\alpha)\pi)}{\pi}. \tag{55}$$

Equations (54) and (55) demonstrate the dependence of the mass ablation rate, for a single wire in a heat bath, on all variables of the system, namely, the asymptotic temperature of the bath T_0, the wire size r_w, and the properties of the density profile ρ_0, μ, and s. In the case $\mu(m-\alpha)>1$, the dependence on the parameter ϵ, which we must regard as small but finite, is troubling, and Eq. (54) cannot be used to predict absolute values of the ablation rate. Nonetheless we hope that the predicted *scalings* with ρ_0, T_0, r_w are correct. The dependence on ϵ in Eq. (54) can be traced back to the singular nature of the integral, Eq. (53), as $\epsilon \to 0$. To illustrate, for $0<\mu(m-\alpha)<1$, the integral is well-behaved as $\epsilon \to 0$ [see Eq. (50)], and consequently $\tilde{\dot{m}}$, expressed in Eq. (55), is independent of ϵ.

V. COMPARISON TO SIMULATION

We have described in the previous section a 1D (radial), steady-state model for wire ablation, namely, a single wire ablating (due to radiation transport) in an infinitely large heat bath with asymptotic temperature T_0. We hope that such a description is relevant to the much more complicated problem of a wire ablating in a wire array. Note that for our model to be applicable, the mass ablation rate must be driven by physics in a region close to the wire core, where flow is still cylindrically symmetric, and the global $\mathbf{j} \times \mathbf{B}$ has not yet broken this symmetry. To test the validity of our model, we compare the prediction of the final result of our theory, namely, Eq. (54), with the results of simulation.

At this point we simplify Eq. (54) by setting the exponents for the enthalpy and radiation mean free path, as defined in Eqs. (35) and (36), to $m=-0.14$, $n=1.6$, $\alpha=-1.3$, $\beta=1.5$, as in Ref. 18. Note that such fits appear to be in excellent agreement with simulation. We also set $\gamma=0.6$, where γ was defined in Eq. (43), once again in accord with simulation. Finally, as will be shown to be the case later, we assume that Eq. (47) is a good fit to the simulation density profile, with a *fixed* value of μ, i.e., $\mu=1.1$. Consequently, $\mu(m-\alpha)=1.276>1$ and Eq. (54) yields the scaling relation

$$\dot{m} \propto \frac{T_0^{2.3} r_w}{\rho_0^{1.16}}. \tag{56}$$

Note that in the above equation we have omitted the dependence on ϵ and s, which are regarded as fixed.

The two major results we would like to extract from Eq. (56) are the scaling of the mass ablation rate $\dot{m}$ with wire size r_w and wire number N. However, in general both ρ_0 and T_0 will vary with r_w and N, and this exact dependence cannot be predicted by our simple model. Consequently, our aim will be to simply test the validity of Eq. (56). Namely, we will determine the dependence of T_0 and ρ_0 on r_w and N via simulation, and then compare the resulting scaling of $\dot{m}$, as determined by Eq. (56), with simulation results. If our simple model, embodied in Eq. (56), is indeed an adequate approximation to the more complicated physics being modeled in the simulation, then the scaling of ablation rate as determined by Eq. (56) and simulation should agree.

A. Scaling with r_w

We will first use Eq. (56) to predict how $\dot{m}$ varies with r_w, leaving all other array parameters fixed. As mentioned earlier, we cannot say that Eq. (56) predicts $\dot{m}$ varies linearly with r_w, because T_0 and ρ_0 are also functions of r_w. Our model described in Sec. IV assumes a wire ablating in a large heat bath, with boundary condition $T(r \to \infty)=T_0$. In order

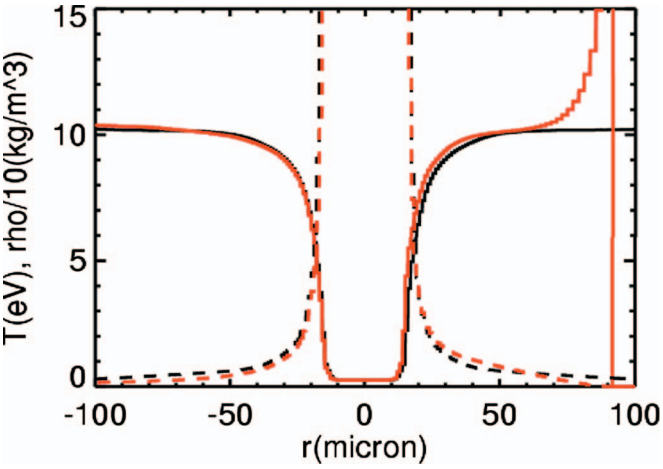

FIG. 8. (Color) Lineout through the center of the core of T (solid) and $\rho/10$ (dashed) in x (red) and y (black) directions, for $N=100$, $r_w=15$ μm, $I=3$ MA. The fact that the profiles nearly overlay suggests a region of cylindrical symmetry about the wire, up to 70 μm.

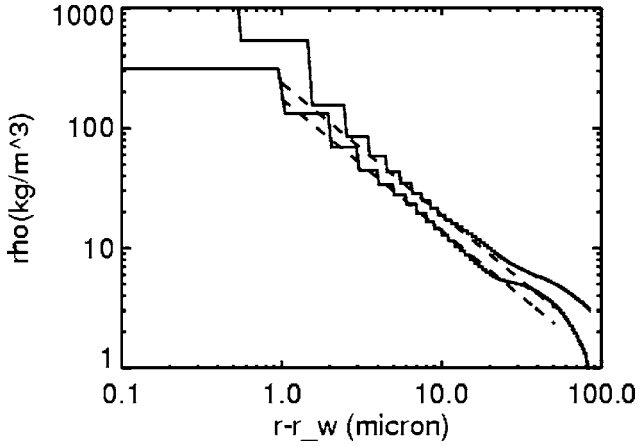

FIG. 10. Plot of ρ (kg/m^3) as a function of $r-r_w$ (μm) on the log-log plot, for $r_w=5$ μm (lower solid curve) and $r_w=15$ μm (upper solid curve), in the case $N=100$, $I=3$ MA. Also shown are fits (dashed lines) using Eq. (47), with $\mu=1.1$.

for this model to apply to the wire-array simulation, there must exist in simulations a region of cylindrical symmetry about the core, over which the temperature rapidly increases from a very low value (at the core surface), to its asymptotic value T_0. We would expect that as we decrease the spacing between wires in the array geometry, the spacing eventually becomes so small that this cylindrically symmetric region cannot exist, as is certainly the case in the limit in which the cores are touching (i.e., shell limit). With this in mind, so as not to stress the limits of our model, we first consider a relatively low wire number case, $N=100$, with relatively large interwire gaps. Indeed if we plot ρ and T profiles along the x and y directions (see Fig. 2 for orientation of x-y axes) through the center of the core, we see a region of cylindrical symmetry about the core (see Fig. 8). Note that the temperature reaches its asymptotic value T_0 within this cylindrically symmetric region.

In addition to symmetry, another assumption in the derivation is the scaling of T with T_r, i.e., Eq. (43). In Fig. 9 we demonstrate that $\gamma=0.6$ provides a good fit in the region of interest (i.e., $r>r_w$). As discussed earlier, near the core $T<T_r$, which is consistent with radiation heating. Recall that our simple model is based on the assumption that near the core, the dominant heating mechanism is radiation, and the dominant cooling mechanism, required for a steady state, is convective enthalpy flux. Consequently, formally our model can only apply in the region where $T<T_r$, i.e., from $r=r_w=15$ μm to $r=35$ μm. For larger radii, $T>T_r$, implying radiation *cooling*. Hence, out here Joule heating now plays the role of the dominant heating mechanism, and the crux of our model, namely, the simple energy balance, Eq. (31), no longer holds.

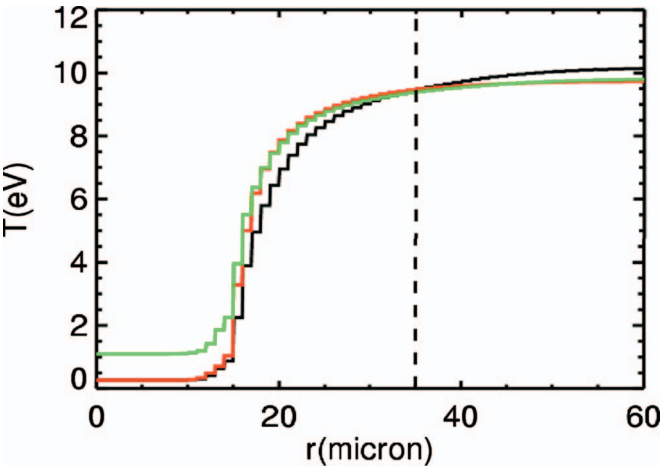

FIG. 9. (Color) Lineout of T (eV) (black), T_r (red), and $T_{r,\mathrm{fit}}=103T^{0.6}$ (green), for $N=100$, $r_w=15$ μm, $I=3$ MA. The dashed vertical line separates regions of radiation heating and cooling.

In Fig. 10 we plot $\rho(r-r_w)$ for two values of r_w, on a log-log plot. Note that if ρ is described by Eq. (47),

$$\ln\rho=\ln\rho_0+\mu\ln s-\mu\ln(r-r_w), \tag{57}$$

then a plot of $\ln\rho$ vs $\ln(r-r_w)$ will generate a straight line with slope $-\mu$. Indeed the plots reveal that a straight line fit, with $\mu=1.1$ is accurate, and in fact the slope μ appears to be an invariant of r_w.

Now, ρ_0, defined as the density at a distance $s=10$ μm from the core surface, is a slowly varying function of r_w, as can be seen in Fig. 11. Note that the core boundary, r_w, is usually easily identified by an order of magnitude drop in density as we move from core to corona. However, the 1 μm cell resolution introduces an uncertainty into the exact location of r_w, which in turn translates into a significant uncertainty in ρ_0, due to the steepness of the density profile near the core. In Fig. 11 we provide error bars to emphasize the point that although $\rho_0\sim r_w^{0.3}$ yields a good fit, the measurement of ρ_0 is imprecise, and really simulations should be run with finer resolution to reduce the uncertainty in ρ_0.

Also, in Fig. 11 we demonstrate that T_0 is a slowly decreasing function of r_w. This is consistent with our previous observation that the coronal density is increasing with r_w, coupled with our scaling relation (16) $h\sim B^2/\mu_0\rho$.

With these scalings for ρ_0 and T_0, Eq. (56) predicts the following scaling for the mass ablation rate with wire size:

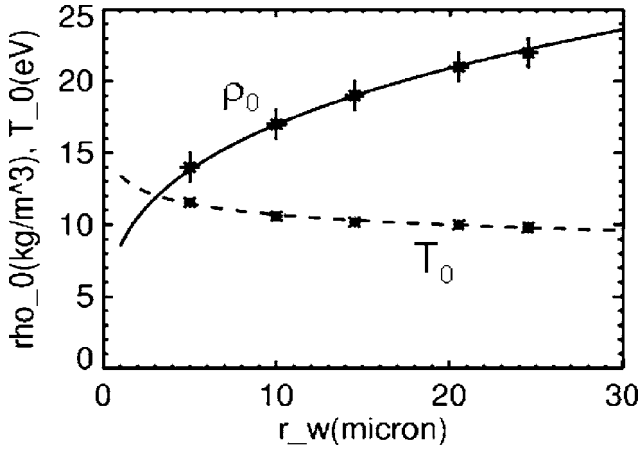

FIG. 11. Plot of ρ_0 (upper crosses) and T_0 (lower crosses), as determined by simulation, as a function of r_w (μm) for $N=100$, $I=3$ MA. The dashed line is $T_0 \sim r_w^{-0.1}$, while the solid line is $\rho_0 \sim r_w^{0.3}$.

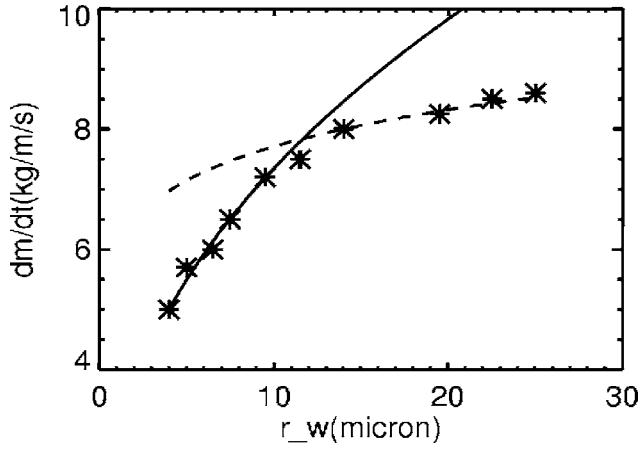

FIG. 13. Plot of $\dot{m}$ (kg/m/s) vs r_w (μm) for $N=300$, $I=3$ MA. The crosses represent the steady-state values of $\dot{m}$ obtained from simulation. The solid line is $\dot{m} \sim r_w^{0.42}$, while the dashed line is $\dot{m} \sim r_w^{0.11}$.

$$\dot{m} \sim r_w^{2.3(-0.1)+1-1.16(0.3)} \sim r_w^{0.42}. \tag{58}$$

The steady-state values of the ablation rate, as determined from simulation, are plotted in Fig. 12, along with the prediction of our theory, $\dot{m} \sim r_w^{0.42}$. The agreement between the two suggests that our simple model of ablation is an adequate description of the physics in the simulation.

Having found that our simple model appears applicable to the $N=100$ case, we now consider a higher wire number case, $N=300$, which, lying closer to the shell-like limit, will stress the assumptions of our model. In Fig. 13 we plot $\dot{m}(r_w)$. Note that unlike the $N=100$ case, $\dot{m}$ appears to exhibit two different scalings, depending on whether r_w is greater or less than, roughly speaking, 12 μm, which corresponds to a core diameter to the interwire gap ratio $d/\Delta \sim 0.11$; here $\Delta \equiv 2\pi R_0/N$.

The appearance of two different scaling regimes in $\dot{m}$ is reflected in $\rho_0(r_w)$ and $T_0(r_w)$, plotted in Fig. 14. Error bars on ρ_0 should be included here, as in Fig. 11, but are omitted in the interest of clarity. For $r_w < 12$ μm, we can fit $\rho_0 \sim r_w^{0.3}$ and $T_0 \sim r_w^{-0.1}$ (which are the same scaling relations found for $N=100$), whereas for $r_w > 12$ μm, $\rho_0 \sim r_w^{0.45}$ and $T_0 \sim r_w^{-0.16}$. From Eq. (56), our simple model would predict that for $r_w < 12$ μm, $\dot{m} \sim r_w^{0.42}$, and for $r_w > 12$ μm, the scaling is far weaker, $\dot{m} \sim r_w^{0.11}$. These fits are plotted in Fig. 13 and once again appear in good agreement with simulation results, implying that even in this high wire number case, our simple model applies.

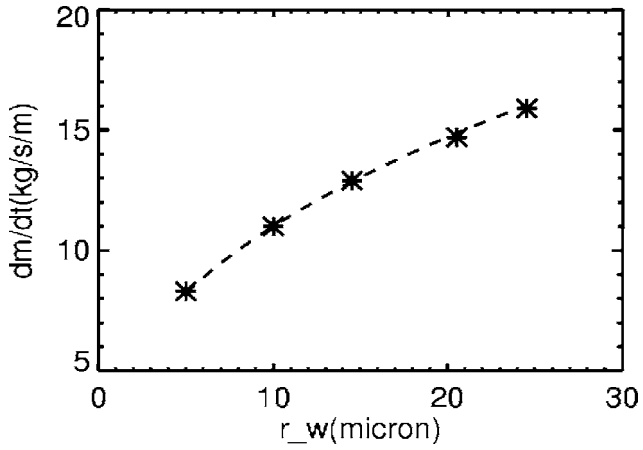

FIG. 12. Plot of $\dot{m}$ vs r_w for $N=100$, $I=3$ MA. The crosses represent the steady-state values of $\dot{m}$ obtained from simulation. The dashed line represents $\dot{m} \sim r_w^{0.42}$, the scaling predicted by Eq. (58).

In the limit $d/\Delta \to 1$, wire cores touch and the wire array transitions to a purely one-dimensional (1D) shell, in which case $\dot{m}$ is independent of r_w. We postulate that the weak dependence of $\dot{m}$ on r_w for $d/\Delta > 0.11$ is a reflection of this transition to the shell-like limit. That the transition to 1D occurs for such a small value of d/Δ is not too surprising. For instance, in the case of an array of current-carrying plasma columns of diameter D, when the column size to gap ratio D/Δ exceeds the critical value $1/\pi$, magnetic field lines can no longer penetrate through gaps between the columns.[45] Consequently in this case the magnetic field distribution is effectively 1D in the sense that it is equivalent to that of a perfectly conducting shell.

In our case, current is not constrained to flow in well-defined columns, but rather distributes itself throughout the interwire gap. Therefore, perhaps a more appropriate condition for the transition to 1D may be found in Ref. 46, where it is argued that the transition occurs, roughly speaking, when $\delta/\Delta > 1$ (recall δ is the resistive layer width). Such a viewpoint is not in contradiction to the simulations if we define the magnetic Reynold's number as the ratio of inductive and resistive terms in the electric field [cf. Eq. (1)], $R'_M = vB/\eta j$ [note that in the approximation $j \sim B/\mu_0\delta$, $R'_M \sim \mu_0 v\delta/\eta$, exactly as in our previous definition for the magnetic Reynold's number R_M, Eq. (3)]. As before, we can estimate the size of the resistive layer δ as the location where $R'_M \sim 1$ [cf. Eq. (4)], or equivalently where $vB \sim \eta j$. Before continuing we point out that such a definition for δ, which is that used in Ref. 46, yields values smaller (by a factor of about 5) than that using Eq. (4). The discrepancy can be traced to the fact that rather than $j \sim B/\mu_0\delta$, more accurately $j \sim \delta B/\mu_0\delta$, where δB is the change in B associated with length scale δ. It follows that $R'_M \sim (\mu_0 v\delta/\eta)(B/\delta B)$

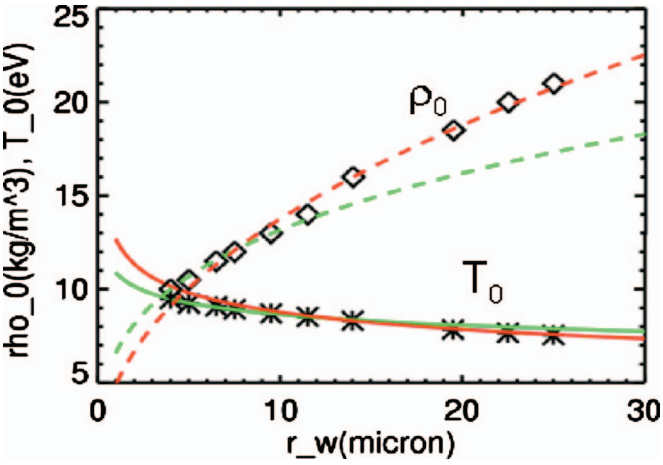

FIG. 14. (Color) Plot of ρ_0 (kg/m^3) (diamonds) and T_0 (eV) (crosses) as a function of r_w (μm) for $N=300$, $I=3$ MA. We plot $\rho_0 \sim r_w^{0.3}$ (dashed green line) and $T_0 \sim r_w^{-0.1}$ (solid green), appropriate for $r_w < 12$ μm, and also $\rho_0 \sim r_w^{0.45}$ (dashed red) and $T_0 \sim r_w^{-0.16}$ (solid red), appropriate for $r_w > 12$ μm.

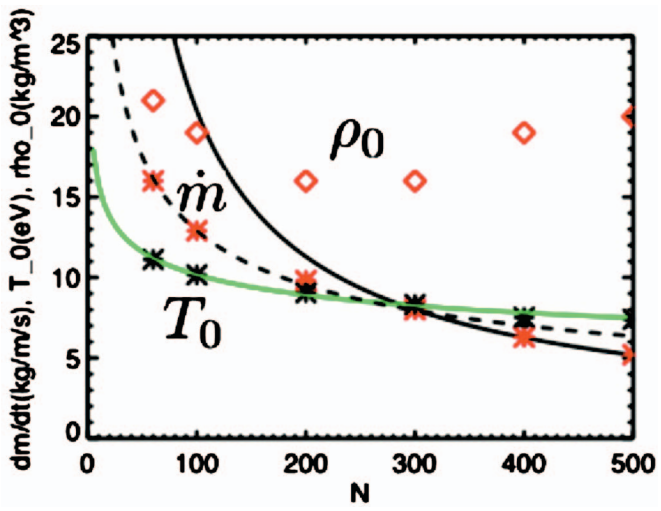

FIG. 15. (Color) $\dot{m}$ (kg/m/s) (red crosses), T_0 (eV) (black crosses), and ρ_0 (kg/m^3) (red diamonds) vs N for $r_w=15$ μm, $I=3$ MA. We plot $\dot{m} \sim N^{-0.44}$ (black dashed), $\dot{m} \sim N^{-0.85}$ (black solid) and $T_0 \sim N^{-0.19}$ (green).

$\sim R_M B/\delta B$. For a typical δ calculated using $vB \sim \eta j$, $\delta B/B \sim 1/5$, thereby accounting for the aforementioned factor of 5 difference in length scale. Calculating δ using the condition $\eta j \sim vB$, we find that in the case $N=300$, $I=3$ MA, as we increase r_w from 5 μm to 25 μm, δ increases from 50 μm to 250 μm, suggesting that in between these limits the wire array satisfies $\delta \sim \Delta (=209$ μm) and therefore transitions to the 1D scaling, in accord with Fig. 13.

In Table I, we summarize the results of our r_w scan, for various values of N. Here, the scaling for $\dot{m}$ is obtained from Eq. (56), and for all values of N, the predicted scaling agrees well with that found from simulation. We observed a single ablation rate scaling for $N=60$ and $N=100$, but the interwire gaps are so large in these cases that we only explored very small values of d/Δ (the maximum values of d/Δ sampled for $N=60$ and $N=100$ were 0.057 and 0.08, respectively). For $N>100$, the ablation rate scaling exhibits multiple scaling, depending on the value of d/Δ. Note that the "critical value" of d/Δ at which the scaling changes, is only meant to be taken as a rough estimate. In any case, we observe that for d/Δ small enough, the scaling of $\dot{m}$, ρ_0, and T_0 all appear fairly independent of N, and satisfy, roughly speaking, $\dot{m} \sim r_w^{0.4}$, $T_0 \sim r_w^{-0.1}$, $\rho_0 \sim r_w^{0.3}$. For larger values of d/Δ, the scaling of ρ_0 and T_0 are modified such as to reduce the scaling of $\dot{m}$ with r_w.

TABLE I. Scaling of $\dot{m}$ with r_w, for $I=3$ MA, $R_0=0.01$ m.

N	$\dot{m} \sim r_w^a$ a	$T_0 \sim r_w^{-b}$ b	$\rho_0 \sim r_w^c$ c
60	0.41	0.13	0.25
100	0.42	0.1	0.3
200 ($d/\Delta<0.13$)	0.42	0.1	0.3
200 ($d/\Delta>0.13$)	0.31	0.1	0.4
300 ($d/\Delta<0.11$)	0.42	0.1	0.3
300 ($d/\Delta>0.11$)	0.11	0.16	0.45
400 ($d/\Delta>0.13$)	0.13	0.15	0.45

B. Scaling with *N*

Now we wish to address the question of how $\dot{m}$ scales with wire number N, keeping all other array parameters fixed. Once again, from Eq. (56), we must determine how the asymptotic temperature T_0 and characteristic density ρ_0 scale with N. These quantities are plotted in Fig. 15, for a fixed value of $r_w=15$ μm. While $T_0 \sim N^{-0.19}$ yields a good fit, $\rho_0(N)$ is not monotonic, and consequently we cannot use a simple power law fit. Note, however, that if we assume ρ_0 independent of N, then Eq. (56) predicts $\dot{m} \sim N^{-(0.19)2.3} \sim N^{-0.44}$, which from the figure appears to be a good prediction over N ranging from 60 to 300. For $N>300$, however, which corresponds to $d/\Delta>0.14$, $\dot{m}$ scales more strongly with N: $\dot{m} \sim N^{-0.85}$.

VI. COMPARISON TO EXPERIMENT

Let us now investigate the relevance of these steady-state simulations to experiment, which are of course time varying. To this end we introduce Lebedev's "rocket model,"[13] which assumes that the current is concentrated in a thin layer near the wire cores. The $\mathbf{j}\times\mathbf{B}$ force acting in the layer rapidly accelerates plasma towards the array axis until, at the layer edge, plasma exhausts at an "ablation velocity" v_{abl}. Consequently, momentum balance yields a rocket-like equation:

$$\dot{m}_{\mathrm{total}} v_{\mathrm{abl}} = -\frac{\mu_0 I^2}{4\pi R_0}. \tag{59}$$

Note that Eq. (59) is equivalent to Eq. (8), since $\dot{m}_{\mathrm{total}} = -2\pi\rho v R_0$. As shown in Fig. 16 (originally published in Ref. 27), Lebedev has inferred from experimental data, taken on the 1 MA MAGPIE facility at Imperial College, a dependence of v_{abl} on the ratio Δ/d, where $\Delta \equiv 2\pi R_0/N$ is the interwire gap and d is the core diameter. Note that d is measured from radiography and represents the size of the dense ablating core. In general it will be significantly larger than the original wire diameter d_0, because the core is actually

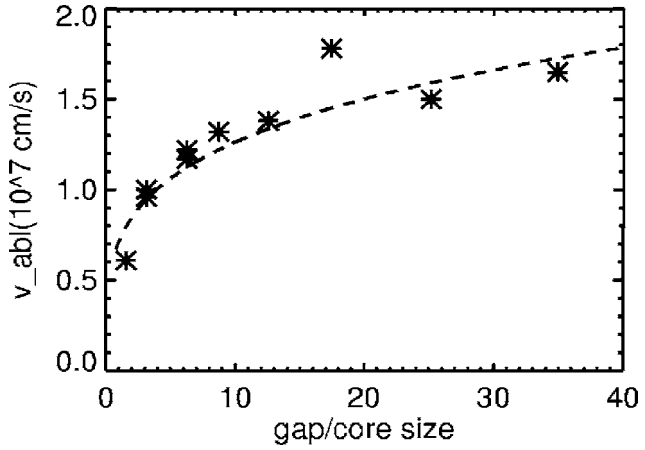

FIG. 16. Variation of v_{abl} with the ratio of gap to core size, Δ/d, as determined by experimental data (courtesy of S. Lebedev). Also shown is the fit $v_{\mathrm{abl}} \sim (\Delta/d)^{0.25}$.

slowly expanding at the sound speed, due to the Joule energy deposited in the core prior to corona formation. In contrast, in our simulations $d \sim d_0$, because we initialize cores at low temperature, and suppress any subsequent Joule heating (see Sec. II).

Now, the fundamental quantity measured in simulation is not v_{abl}, but rather $\dot{m}_{\mathrm{total}}$, the total ablation rate of the array, i.e., $\dot{m}_{\mathrm{total}}=N\dot{m}$, where $\dot{m}$ is the ablation rate of a single wire in the array. The variation of $\dot{m}_{\mathrm{total}}$ with d/Δ is shown in Fig. 17. To relate $\dot{m}_{\mathrm{total}}$ to v_{abl} we note that Eq. (59) suggests that if I and R_0 are held fixed, as is the case in all simulations shown in Fig. 17, then $v_{\mathrm{abl}} \sim 1/\dot{m}_{\mathrm{total}}$. Consequently, if $\dot{m}_{\mathrm{total}} \sim (d/\Delta)^{\alpha}$, then $v_{\mathrm{abl}} \sim (\Delta/d)^{\alpha}$. In Figs. 16 and 17 we plot such a fit for $\alpha=0.25$ and demonstrate reasonable agreement between simulation and experimental trends. Because of uncertainties in the rigor of comparison between simulation and experimental results, however, we emphasize only the qualitative agreement, namely, weak and monotonic dependence of $\dot{m}_{\mathrm{total}}$ (or v_{abl}) on d/Δ.

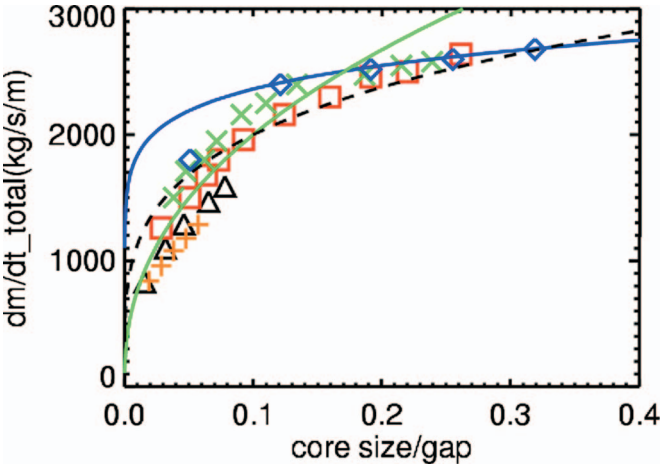

FIG. 17. (Color) Variation of $\dot{m}_{\mathrm{total}}$ with the ratio of core size to interwire gap, d/Δ, as determined from simulation, for $I=3$ MA and $R_0=0.01$ m. Shown are the results for $N=60$ (+), $N=100$ (△), $N=200$ (□), $N=300$ (×), and $N=400$ (◇). Also shown are the fits $\dot{m}_{\mathrm{total}} \sim (d/\Delta)^{0.25}$ (dashed), $\dot{m}_{\mathrm{total}} \sim (d/\Delta)^{0.42}$ (green), and $\dot{m}_{\mathrm{total}} \sim (d/\Delta)^{0.11}$ (blue).

Recall from the simulation results of Sec. V that in general $\dot{m}$ exhibits two branches of solution, depending on the value of d/Δ, which we attributed to a transition to the 1D shell-like limit. Roughly speaking, for $d/\Delta<0.1$, $\dot{m} \sim N^{-0.44} r_w^{0.42}$, implying

$$\dot{m}_{\mathrm{total}} = N\dot{m} \sim N^{0.56} r_w^{0.42} \sim \left(\frac{d}{\Delta}\right)^{0.42} N^{0.14}, \tag{60}$$

whereas in the opposite limit $d/\Delta>0.1$, $\dot{m} \sim N^{-0.85} r_w^{0.11}$, so that

$$\dot{m}_{\mathrm{total}} \sim N^{0.15} r_w^{0.11} \sim \left(\frac{d}{\Delta}\right)^{0.11} N^{0.04}. \tag{61}$$

There are several interesting points to extract from these expressions. In the case $d/\Delta>0.1$, the extremely weak dependence on N in Eq. (61) implies that $\dot{m}_{\mathrm{total}}$ is a function mainly of d/Δ, in agreement with Fig. 17. In contrast, for $d/\Delta<0.1$, Eq. (60) predicts $\dot{m}_{\mathrm{total}}$ is not only a more strongly varying function of d/Δ [i.e., $\dot{m}_{\mathrm{total}} \sim (d/\Delta)^{0.42}$, plotted in Fig. 17], but also exhibits a non-negligible dependence on N, for fixed d/Δ. Indeed, in the case $d/\Delta<0.1$, Fig. 17 demonstrates that for fixed d/Δ, $\dot{m}_{\mathrm{total}}$ increases with N, qualitatively in accord with Eq. (60) (although $N^{0.22}$ appears to be a better fit than $N^{0.14}$).

Recently Sinars[25] has inferred from radiographic measurements, taken on the 20 MA Z facility at Sandia National Laboratories, that $\dot{m}_{\mathrm{total}}$ increases with core diameter d ($N=300$ and $R_0=0.01$ m were held fixed in these experiments). Cuneo[26,47] has attempted to quantify this dependence. Using "small" wires ($d_0<12$ μm), he finds $\dot{m}_{\mathrm{total}} \sim d_0^{\alpha}$, where α lies between 0.66 and 0.92, which is considerably stronger than our scaling obtained from the steady-state simulation $\dot{m}_{\mathrm{total}} \sim d^{0.42}$ (recall that in our simulations $d \sim d_0$).

A natural question to address at this point is the relevance of the steady-state analysis to the actual time-varying case. If the time scale on which equilibrium is reached is short compared to that on which the current I varies, then the system might reach a quasiequilibrium. The mass ablation rate is determined by physics within the resistive layer. Consequently we expect that equilibrium within the layer is established on either a convective time scale, $\tau_{\mathrm{convect}} \sim \delta/v$, or magnetic diffusive time scale, $\tau_{\mathrm{diffuse}} \sim \mu_0 \delta^2/\eta$, where δ is the resistive layer width. Since the layer width is defined by $R_M=1$ (which we recall signifies that magnetic diffusion and convection are of equal strength in the resistive layer), the two time scales are in fact the same

$$\tau_{\mathrm{diffuse}} \sim \frac{\mu_0 \delta}{\eta} \frac{\eta}{\mu_0 v} \sim \frac{\delta}{v} \sim \tau_{\mathrm{convect}} \equiv \tau, \tag{62}$$

where we have used Eq. (4). For $N=300$, $I=3$MA, $r_w=15$ μm, $R_0=0.01$ m, typically $v \sim 2.5\times10^4$ m/s and $\eta \sim 1.6\times10^{-5}$ Ω m, yielding $\tau \sim \eta/\mu_0 v^2 \sim 20$ ns. Note from Fig. 6 that for these same array parameters the actual time taken for $\dot{m}$ to reach equilibrium is about 160 ns, or 8τ.

In general $\tau \sim \eta/\mu_0 v^2$ will vary significantly with N, r_w, and I. Geometrically we can reduce τ by decreasing the core size to gap ratio $d/\Delta \sim r_w N$, which will decrease the characteristic ρ in the resistive layer and consequently increase v

(since in equilibrium $\rho v R$ is a spatial constant, by mass conservation). We can also reduce τ by increasing I, which will increase v [see Eq. (27)] while decreasing η.

Preliminary studies show that the steady-state scaling relations, when applied to ablation rates obtained using (r,θ) simulations driven with a time-dependent Z current drive, predict quite well the variation of $\dot{m}$ with r_w and I, so long as $I<6$ MA. However, at larger currents, $\dot{m}$ scales more strongly with both r_w and I than predicted by our steady-state scaling relation $\dot{m}\sim r_w^{0.42}I^{1.4}$, as shown in Eq. (60) and Fig. 7 (which is perhaps not surprising since the r_w scaling was obtained with a fixed "low" value of current, $I=3$ MA). This observation is in accord with the previously mentioned experimental finding by Cuneo, and its explanation and implications require further study.

VII. CONCLUSIONS

We have observed from simulation that, close to the core, a cylindrically symmetric region exists where the steady-state ablation physics can be distilled into a very simple balance between convective cooling and radiation heating. This observation has permitted us to construct a very simple model which predicts the scaling of ablation rate as a function of the coronal temperature as well as properties of the density profile. The final result, Eq. (56), depends on quite a few assumptions, sometimes even of a conflicting nature! For instance, the model assumes the validity of the radiation diffusion approximation, which holds in the limit in which the resistive layer is optically thick, and is thus better suited to small interwire gaps Δ. This condition is at odds with the requirement that a region of cylindrical symmetry exist about the core, as discussed in Sec. V A. Furthermore, Eq. (56) relies on the *ad hoc* density profile equation (47), supported by simulation, as well as multiple power law fits to the enthalpy [cf. Eq. (35), valid for tungsten], photon mean free path [cf. Eq. (36), again valid for tungsten], and radiation temperature [Eq. (43)].

Given that our model depends fairly sensitively on the exponents used in these assumptions, Eq. (56), and especially the values of the exponents appearing here, must be taken with caution. Having said all this, the model appears to predict a scaling of ablation rate with wire core radius r_w that is in accord with simulation, over a wide range of wire number N, and the simulations, in turn, are not in contradiction to the experimentally inferred scaling of mass ablation rate with d/Δ. Our simulations reveal that the mass ablation rate scales differently, as described by Eqs. (60) and (61), depending on the value of d/Δ.

Primarily our goal has been twofold: first, to elucidate the physics of the resistive layer governing ablation, as embodied in Eqs. (4), (9), (16), and (22), and second, to isolate the dominant physics governing core ablation, thereby paving the way for a 1D (cylindrical) analytical model that can help explain the dependence of ablation rate on wire size. In order for the model to become experimentally relevant, we must relate its parameters ρ_0 ("characteristic" density) and T_0 ("characteristic" temperature) to the experimental parameters I,N,R_0,r_w. Also, we must better understand the relevance of the steady-state analysis to the actual time-varying situation. Related to this topic is the fact that we assume an unexpanded, stationary core, when in reality the core consists of an expanded liquid droplet/vapor mixture, slowly expanding at the sound speed. Finally, we have restricted our analysis of the ablation process to the (r,θ) plane, when in fact the process is 3D in nature. To be more specific, the wire cores are known to ablate axially nonuniformly, due to an axial instability (the origin of which is still unknown, but is possibly electrothermal in nature[48]). Nonetheless, despite the limitations of our analysis, we hope that the work presented here will be of benefit to the understanding of wire core ablation in the Z pinch.

ACKNOWLEDGMENTS

E.P.Y. would like to thank R. Vesey, T. Mattsson, E. Waisman, R. Lemke, M. Desjarlais, and S. Slutz at Sandia National Labs, and J. Chittenden at Imperial College, for helpful discussions. Thanks also to the ALEGRA-HEDP team: T. Brunner, T. Haill, H. Hanshaw, C. Garasi, A. Robinson, and K. Cochrane.

Sandia is a multiprogram laboratory operated by Sandia Corporation, a Lockheed Martin Company, for the National Nuclear Security Administration under Contract No. DE-AC04-94AL85000.

APPENDIX: THERMAL CONDUCTION VS RADIATION TRANSPORT

Here we wish to estimate the relative importance of energy flux to the core due to electron thermal conduction and radiation transport. The electron-ion and ion-ion collision times are written (see, for instance, Ref. 49)

$$\tau_{ei}\sim\frac{6\sqrt{2}\pi^{3/2}\epsilon_0^2 m^{1/2}(k_bT_e)^{3/2}}{n_iZ^2e^4\ln\Lambda} \tag{A1}$$

and

$$\tau_{ii}\sim\frac{12\pi^{3/2}\epsilon_0^2 M^{1/2}(k_bT_i)^{3/2}}{n_iZ^4e^4\ln\Lambda}, \tag{A2}$$

respectively. Here n_i is the ion number density, $m(M)$ is the electron (ion) mass, $T_e(T_i)$ is the electron (ion) temperature, Z is the ionization state of the plasma, $\ln\Lambda$ is the Coulomb logarithm, and k_b is Boltzmann's constant. All units are SI. Recalling the definition of the electron cyclotron frequency $\Omega_e=eB/m$ and ion cyclotron frequency $\Omega_i=eB/M$, we find that

$$\Omega_e\tau_{ei},\Omega_i\tau_{ii}\ll 1 \tag{A3}$$

for typical tungsten plasma corona conditions near the core, i.e., $n_i\sim 1\times10^{26}/\mathrm{m}^3$, $Z\sim4$, $T_e\sim T_i\sim T\sim 8\times10^4$ K, $\ln\Lambda\sim5$, $B\sim100$ T. Assuming $T_e\sim T_i$ is reasonable, because for the typical coronal values listed above, the temperature equilibration time $\tau_{\mathrm{eq}}\simeq(M/2m)\tau_{ei}\simeq0.05$ ns, which is short compared to the ns time scale associated with most Z-pinch generators. Equation (A3) implies that ions and electrons are *unmagnetized*. In this limit, thermal conduction is dominated by electron thermal conduction, so that in the heat flux vector

$$\mathbf{q} = -\kappa \nabla T, \tag{A4}$$

we have

$$\kappa \simeq \kappa_e = \frac{K^C n_e k_b^2 T \tau_{ei}}{m}. \tag{A5}$$

Here K^C is a dimensionless function of Z and has been tabulated by Epperlein and Haines[50] (for $Z=4$, $K^C \simeq 7$).

We now employ the radiation heat conduction approximation, which assumes the radiation energy density is Planckian $U \simeq U_p$ and consequently, from Eqs. (33) and (39),

$$\mathbf{S} \simeq -\kappa_{\mathrm{rad}} \nabla T, \tag{A6}$$

where

$$\kappa_{\mathrm{rad}} = \frac{16\sigma l T^3}{3}. \tag{A7}$$

Although this approximation is actually invalid in the context of our simple ablation model, as pointed out in Sec. IV, it nonetheless allows us to make an order of magnitude comparison between radiation and electron heat conduction. The relative importance of the two mechanisms is captured by $\kappa_e/\kappa_{\mathrm{rad}}$, which, combining Eqs. (A1), (A5), and (A7), can be expressed as

$$\frac{\kappa_e}{\kappa_{\mathrm{rad}}} = \frac{9\sqrt{2}\pi^{3/2} k_b^{7/2} \epsilon_0^2 K^C T^{-2} \rho^{1.3}}{8\sigma l_0 \sqrt{m} e^4 \ln \Lambda Z} = \frac{(6.4e6) K^C \rho^{1.3}}{Z T^2 \ln \Lambda}, \tag{A8}$$

where we have used the expression for the Rosseland mean free path $l \sim (3\times 10^{-11})\rho^{-1.3} T^{1.5}$ m, as found in Ref. 18.

For our typical values $\rho \sim n_i M \sim (1\times 10^{26}/\mathrm{m}^3)(184 \times 1.67 \times 10^{-27}\ \mathrm{kg}) \sim 30\ \mathrm{kg/m}^3$, $T \sim 8\times 10^4$ K, $\ln \Lambda \sim 5$, $Z \sim 4$, $K^C \sim 7$, we find $\kappa_e/\kappa_{\mathrm{rad}} \sim 3\%$, so that in general radiation conduction dominates over electron thermal conduction. Now, for large enough densities and low enough temperatures (i.e., very close to the core), $\kappa_e \gg \kappa_{\mathrm{rad}}$, breaking the assumption of our model, as noted in Ref. 46. However, there it was found this region is very small ($\sim 1\ \mu$m), and its presence is not expected to significantly alter the analysis of Sec. IV.

[1] T. W. L. Sanford, G. O. Allshouse, B. M. Marder *et al.*, Phys. Rev. Lett. **77**, 5063 (1996).
[2] C. Deeney, M. R. Douglas, R. B. Spielman *et al.*, Phys. Rev. Lett. **81**, 4883 (1998).
[3] R. B. Spielman, C. Deeney, G. A. Chandler *et al.*, Phys. Plasmas **5**, 2105 (1998).
[4] M. K. Matzen, M. A. Sweeney, R. G. Adams *et al.*, Phys. Plasmas **12**, 055503 (2005).
[5] J. H. Hammer, M. Tabak, S. C. Wilks, J. D. Lindl, D. S. Bailey, P. W. Rambo, A. Toor, G. B. Zimmerman, and J. L. Porter, Phys. Plasmas **6**, 2129 (1999).
[6] G. R. Bennett, R. A. Vesey, M. E. Cuneo *et al.*, Phys. Plasmas **10**, 3717 (2003).
[7] R. A. Vesey, M. E. Cuneo, J. L. Porter *et al.*, Phys. Plasmas **10**, 1854 (2003).
[8] T. W. L. Sanford, T. J. Nash, R. E. Olson *et al.*, Plasma Phys. Controlled Fusion **46**, B423 (2004).
[9] S. A. Slutz, J. E. Bailey, G. A. Chandler *et al.*, Phys. Plasmas **10**, 1875 (2003).
[10] J. E. Bailey, G. A. Chandler, S. A. Slutz *et al.*, Phys. Rev. Lett. **92**, 085002 (2004).
[11] S. V. Lebedev, D. Ampleford, A. Ciardi, S. N. Bland, J. P. Chittenden, M. G. Haines, A. Frank, E. G. Blackman, and A. Cunningham, Astrophys. J. **616**, 988 (2004).
[12] S. V. Lebedev, F. N. Beg, S. N. Bland, J. P. Chittenden, A. E. Dangor, M. G. Haines, S. A. Pikuz, and T. A. Shelkovenko, Phys. Rev. Lett. **85**, 98 (2000).
[13] S. V. Lebedev, F. N. Beg, S. N. Bland, J. P. Chittenden, A. E. Dangor, M. G. Haines, K. H. Kwek, S. A. Pikuz, and T. A. Shelkovenko, Phys. Plasmas **8**, 3734 (2001).
[14] V. V. Alexandrov, A. V. Branitskii, G. S. Volkov *et al.*, Plasma Phys. Rep. **27**, 89 (2001).
[15] M. E. Cuneo, E. M. Waisman, S. V. Lebedev *et al.*, Phys. Rev. E **71**, 046406 (2005).
[16] M. E. Cuneo, IEEE Trans. Dielectr. Electr. Insul. **6**, 469 (1999).
[17] L. L. Cowie and C. F. McKee, Astrophys. J. **211**, 135 (1977).
[18] J. D. Lindl, *Inertial Confinement Fusion* (Springer-Verlag, New York, 1998), p. 87.
[19] W. M. Manheimer, D. G. Colombant, and J. H. Gardner, Phys. Fluids **25**, 1644 (1982).
[20] N. Kaiser, J. Meyer-ter-Vehn, and R. Sigel, Phys. Fluids B **1**, 1747 (1989).
[21] S. Atzeni and J. Meyer-ter-Vehn, *The Physics of Inertial Fusion* (Clarendon, Oxford, 2004), p. 196.
[22] M. G. Haines, Plasma Phys. Rep. **29**, 586 (2003).
[23] J. P. Chittenden, S. V. Lebedev, B. V. Oliver, E. P. Yu, and M. E. Cuneo, Phys. Plasmas **11**, 1118 (2004).
[24] E. M. Waisman, M. E. Cuneo, W. A. Stygar, P. V. Sasorov, and E. P. Yu, Phys. Plasmas **13**, 062702 (2006).
[25] D. B. Sinars, M. E. Cuneo, E. P. Yu, S. V. Lebedev, K. R. Cochrane, B. Jones, J. J. McFarlane, T. A. Mehlhorn, J. L. Porter, and D. F. Wenger, Phys. Plasmas **13**, 042704 (2006).
[26] M. E. Cuneo, D. B. Sinars, D. E. Bliss *et al.*, Phys. Rev. Lett. **94**, 225003 (2005).
[27] S. V. Lebedev, D. J. Ampleford, S. N. Bland, S. C. Bott, J. P. Chittenden, C. Jennings, M. G. Haines, J. B. A. Palmer, and J. Rapley, Nucl. Fusion **44**, S215 (2004).
[28] P. Sasorov, *AIP Conference Proceedings, 6th International Conference on Dense Z-Pinches*, Oxford, 2005 (AIP, New York, 2006), No. 808, p. 81.
[29] C. J. Garasi, D. E. Bliss, T. A. Mehlhorn, B. V. Oliver, A. C. Robinson, and G. S. Sarkisov, Phys. Plasmas **11**, 2729 (2004).
[30] A. C. Robinson and C. J. Garasi, Comput. Phys. Commun. **164**, 408 (2004).
[31] R. W. Lemke, M. D. Knudson, A. C. Robinson, T. A. Haill, K. W. Struve, J. R. Asay, and T. A. Mehlhorn, Phys. Plasmas **10**, 1867 (2003).
[32] S. A. Pikuz, T. A. Shelkovenko, D. B. Sinars, J. B. Greenly, Y. S. Dimant, and D. A. Hammer, Phys. Rev. Lett. **83**, 4313 (1999).
[33] G. S. Sarkisov, P. V. Sasorov, K. W. Struve, and D. H. McDaniel, J. Appl. Phys. **96**, 1674 (2004).
[34] G. I. Kerley (private communication, 2000).
[35] M. P. Desjarlais, J. D. Kress, and L. A. Collins, Phys. Rev. E **66**, 025401(R) (2002).
[36] D. B. Sinars, M. E. Cuneo, E. P. Yu, D. E. Bliss, T. J. Nash, J. L. Porter, C. Deeney, M. G. Mazarakis, G. S. Sarkisov, and D. F. Wenger, Phys. Rev. Lett. **93**, 145002 (2004).
[37] S. Kirkpatrick, Rev. Mod. Phys. **45**, 574 (1973).
[38] B. V. Oliver and T. A. Mehlhorn, IEEE Trans. Plasma Sci. **30**, 517 (2002).
[39] M. G. Haines and W. B. Thompson, *Propagation and Instabilities in Plasmas* (Stanford University Press, Stanford, 1963), p. 115.
[40] B. V. Oliver, C. J. Garasi, T. A. Mehlhorn, and E. P. Yu, Bull. Am. Phys. Soc. **47**, 243 (2002).
[41] M. G. Haines, IEEE Trans. Plasma Sci. **30**, 588 (2002).
[42] Y. B. Zel'dovich and Y. P. Raizer, *Physics of Shock Waves and High-Temperature Hydrodynamic Phenomena* (Academic, New York, 1966), pp. 148, 154.
[43] I. S. Gradshteyn and I. M. Ryzhik, *Table of Integrals, Series, and Products*, 5th ed. (Academic, San Diego, 1994), p. 334.
[44] M. Abramowitz and I. A. Stegun, *Handbook of Mathematical Functions* (Dover, New York, 1972), p. 559.
[45] A. L. Velikovich, I. V. Sokolov, and A. A. Esaulov, Phys. Plasmas **9**, 1366 (2002).
[46] P. V. Sasorov, B. V. Oliver, E. P. Yu, and T. A. Mehlhorn, "1D ablation in multiwire arrays" (unpublished).
[47] M. E. Cuneo (private communication, 2005).
[48] M. G. Haines, Phys. Rev. Lett. **47**, 917 (1981).
[49] R. J. Goldston and P. H. Rutherford, *Introduction to Plasma Physics* (Institute of Physics, Bristol, 1995), p. 172.
[50] E. M. Epperlein and M. G. Haines, Phys. Fluids **29**, 1029 (1986).